Pore Network Modeling of Catalyst Deactivation By Coking, from Single Site to Particle, During Propane Dehydrogenation

Guanghua Ye, Haizhi Wang, Xuezhi Duan (ID)**, Zhijun Sui and Xinggui Zhou*** (ID)

State Key Laboratory of Chemical Engineering, East China University of Science and Technology, Shanghai, 200237, China

Marc-Olivier Coppens* (ID)

Dept. of Chemical Engineering, University College London, London, WC1E 7JE, U.K.

Weikang Yuan

State Key Laboratory of Chemical Engineering, East China University of Science and Technology, Shanghai, 200237, China

A versatile pore network model is used to study deactivation by coking in a single catalyst particle. This approach allows to gain detailed insights into the progression of deactivation from active site, to pore, and to particle—providing valuable information for catalyst design. The model is applied to investigate deactivation by coking during propane dehydrogenation in a Pt-Sn/Al₂O₃ catalyst particle. We find that the deactivation process can be separated into two stages when there exist severe diffusion limitation and pore blockage, and the toxicity of coke formed in the later stage is much stronger than of coke formed in the early stage. The reaction temperature and composition change the coking rate and apparent reaction rate, informed by the kinetics, but, remarkably, they do not change the capacity for a catalyst particle to accommodate coke. Conversely, the pore network structure significantly affects the capacity to contain coke. © 2018 The Authors. AIChE Journal published by Wiley Periodicals, Inc. on behalf of American Institute of Chemical Engineers. AIChE J, 65: 140–150, 2019
Keywords: propane dehydrogenation, deactivation by coking, pore network model, pore blockage, catalyst design

Introduction

Propylene is a key feedstock in the petrochemical industry, which is widely used in the production of many important chemicals (e.g., polypropylene, acrylonitrile, propylene oxide, and cumene).[1,2] Propylene is traditionally produced as a byproduct from steam cracking and fluid catalytic cracking, but these processes cannot satisfy the ever-growing demand for propylene in recent years.[3] Hence, techniques for the purposeful production of propylene (including propane dehydrogenation, Fischer-Tropsch-to-olefins, and methanol-to-olefins) have been developed and commercialized.[4] Among these, propane dehydrogenation is currently one of the most economical, due to the large price gap between propane and propylene.[1]

A major problem during propane dehydrogenation is the fast catalyst deactivation by coke formation. This problem persists in industrial processes. For example, the Pt-Sn/ZnAl₂O₃ catalyst used in the Uhde STAR process is significantly deactivated by coke after 7 h on stream; the CrOₓ/Al₂O₃ catalyst used in the Catofin process should be regenerated after only 12 min.[1,5,6] Hence, it is of great importance to design robust catalysts against deactivation by coke formation for propane dehydrogenation. To achieve such robust catalysts, it is essential to understand coking and deactivation at different length scales.

Froment[7-9] classified catalyst deactivation phenomena associated with coke deposition into three levels: micro-level, meso-level, and macro-level. At the micro-level or the active site level, coke covers active sites and isolates these sites from reactants. At this level, it is essential to understand chemical pathways leading to coke precursors, as well as the interaction of these precursors with active sites. At the meso-level or the particle level, coke narrows and even blocks pores, leading to reduced active sites and enhanced diffusion resistance. Hence, at this level, the effect of the pore network structure on coking and deactivation must be accounted for. Finally, at the macro-level or the reactor level, flow and heat transfer affect coking and deactivation of catalysts packed in the reactor, resulting in transient behavior.

For propane dehydrogenation, coking and deactivation at the active site level and the reactor level were extensively investigated. Many density functional theory calculations[10-13] were performed to probe pathways and mechanisms of coke formation over active sites; some kinetic experiments[14-18] were also conducted to correlate deactivation with coking in a quantitative way. Such studies can guide the rational design of catalysts at the active site level, to screen promoters and tailor

active sites. Fixed bed, moving bed, and fluidized bed reactors have been successfully applied in commercial processes for propane dehydrogenation, and much effort[19-23] has been devoted to exploring coking and deactivation in these reactors. This work has contributed to novel reactor designs, such as two-zone fluidized bed reactors.[20-22]

However, up to now, coking and deactivation at the particle or meso-level during propane dehydrogenation has not been reported in the literature, although the knowledge of this is essential to design the catalyst particle, which includes its pore network structure and active site distribution.[24-26] The process of coking and deactivation in a catalyst particle is very complex. Coke can be nonuniformly distributed through the catalyst particle, and the distribution of coke is largely affected by the pore network structure and reaction conditions.[27-30] Coke narrows and eventually plugs pores during reaction, leading to significant changes in pore network structure.[31-33] Some large pores can be surrounded by plugged pores and then become inaccessible to reactants, which further adds to the complexity of the coking process. In addition, a percolation phenomenon occurs when the fraction of unplugged or open pores drops below a critical threshold, in which the previously connected, particle-spanning cluster of open pores becomes disconnected.[24,30,34,35] In this case, macroscopic properties (e.g., effective diffusivity and the observed reaction rates) would experience a sudden change.[24,30,34] This critical fraction of open pores is known as the percolation threshold.[35] Finally, coke deactivates catalyst particles in several ways, not just by covering active sites; a significant loss in activity can also be caused by the increased diffusion resistance and inaccessible active sites when coke narrows and plugs pores.[27,28,33] Considering the above complications, a proper mathematical model is needed to probe coking and deactivation at the particle level, which is what this article sets out to do.

Continuum and discrete models[34,36] can be used to simulate coking and deactivation in a catalyst particle. Continuum models are characterized by a pseudo-homogeneous description of diffusivities, reaction rates, tortuosity factors, and many other macroscopic properties at a length scale much larger than the dimension of individual pores.[29,30,34] Due to this characteristic, continuum models cannot describe percolation phenomena and their associated impacts on catalyst performance. Zhang and Seaton[37] compared continuum models with discrete models, and they proved that continuum models break down when the pore network is close to a percolation threshold. Examples of discrete models are the Bethe lattice[38] and various pore network models[39,40] to describe both morphology and topology of the pore space in catalyst particles. Moreover, pore network models have been successfully used to describe percolation phenomena in some reaction systems, such as hydrodemetallation,[24,29,30] hydrodesulphurization,[41,42] benzene hydrogenation,[43,44] and deactivation of immobilized glucose isomerase.[40,45,46] Therefore, a pore network model should be used to probe coking and deactivation during propane dehydrogenation in a catalyst particle.

In this work, a pore network model is first proposed to describe the coupled diffusion, reaction, coking, and deactivation processes in a catalyst particle for propane dehydrogenation. With this pore network model, we obtain and analyze representative distributions of coke in the catalyst particle, concentration profiles of reactant and products, and the relation between coke content and apparent reaction rate. Eventually, we probe the effects of coking kinetics, reaction conditions, and pore network structure on coking and deactivation processes in the catalyst particle.

Model Formulation

The proposed pore network model can be divided into three interconnected parts, namely, the pore network, diffusion and reaction, and coking and deactivation. Before introducing these parts, the following important assumptions are made. Pt-Sn/Al$_2$O$_3$ is taken as the model catalyst, as it is a widely used catalyst for propane dehydrogenation in industry. The gradients of temperature and total pressure in the catalyst particle are neglected, which is proven to be reasonable in Supporting Information Figure S1. Only the main reaction and coke formation reaction are considered, as other side reactions, like propane cracking, can be neglected under the relevant reaction conditions for propane dehydrogenation.[1] Coke is assumed to be noncatalytic and its formation is irreversible; the density of coke is set to 1200 kg/m^3, which is within the range reported in the literature.[47,48] Finally, at 1 bar, the gas mixture follows the ideal gas law.

Pore network

The pore space of a catalyst particle is represented by the pore network within a two-dimensional disc domain, as illustrated in Figure 1. Two-dimensional pore networks should be adequate to describe the primary features of the pore structure in real catalyst particles and to investigate the effects of the pore structure on deactivation by coke formation, although the dimensionality of the pore network would quantitatively, but not qualitatively, influence the results.[29] Using two-dimensional pore networks reduces the computational time to within a reasonable limit: it takes several hours to conduct a simulation when using a two-dimensional pore network in this work, while the computational time for the same simulation is about 25 times longer (this is, several days) when using a three-dimensional pore network.

The method for generating the pore network is adopted from the work by Ye et al.,[40] in which more details of this
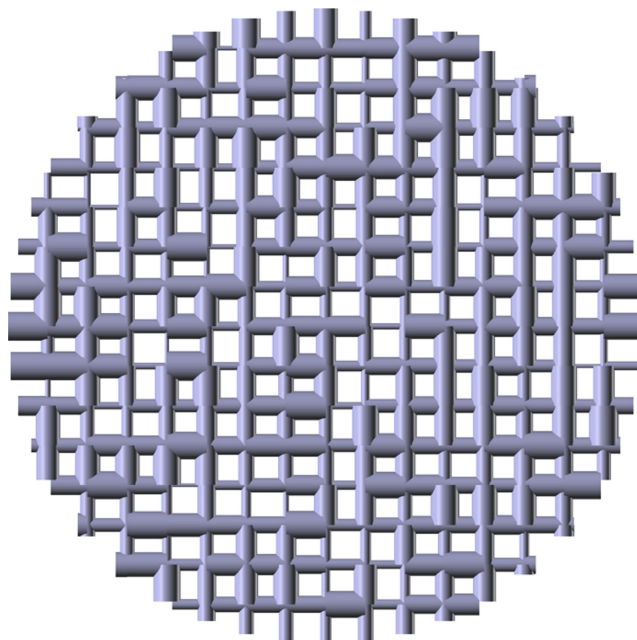

Figure 1. An illustration of the pore network within a disc domain.

In this illustration, the pore connectivity (Z) is 4, and the number of nodes is 253. [Color figure can be viewed at wileyonlinelibrary.com]

method are given. The nodes in the pore network are treated as zero-volume intersections, while the bonds are assumed to be cylindrical pores. The pore connectivity (Z) is kept the same for all inner nodes to simplify the pore network. The original pore radius (r_o) for the fresh catalyst particle is randomly assigned, but follows a log-normal distribution[44]:

$$f(r_o) = \frac{V_t}{\sqrt{2\pi} r_o \sigma} \exp\left[-\frac{(\ln r_o - \ln r_a)^2}{2\sigma^2} \right] \quad (1)$$

Here, V_t is the total pore volume of the catalyst particle, r_a is the volume-averaged pore radius, and σ is the standard deviation of the natural logarithm of the pore radius. The above structural parameters can be obtained from nitrogen sorption and mercury porosimetry measurements.[49]

Diffusion and reaction

In the pore network, the process of diffusion and main reaction can be mathematically described using different equations in pore channels and nodes; the solution of these equations yields concentration profiles of reactant and products. In a pore channel, the diffusion–reaction equation for component i is:

$$\frac{\partial C_i}{\partial t} = -\frac{\partial J_i}{\partial l} + \frac{2r_o R_i}{r^2} \quad (2)$$

where C_i is the concentration of component i, l and r are the length and radius of the pore, J_i is the diffusion flux of component i, and R_i is the reaction rate of component i per unit pore surface area. As, the coking rate is much slower than the rate of diffusion and reaction in this reaction system,[1] the quasi-steady-state condition is satisfied, and Eq. 2 can be simplified to:

$$0 = -\frac{dJ_i}{dl} + \frac{2r_o R_i}{r^2} \quad (3)$$

The diffusion flux (J_i) is described by Fick's law with an effective diffusivity calculated by the Wilke–Bosanquet equation:

$$J_i = -D_{i,e} \frac{dC_i}{dl} \quad (4)$$

$$D_{i,e} = \frac{D_{i,M} D_{i,K}}{D_{i,M} + D_{i,K}} \quad (5)$$

$$D_{i,M} = \frac{1 - x_i}{\sum_{\substack{i=1 \\ j \neq i}}^{n} \frac{x_j}{D_{i,j}}} \quad (6)$$

Here, $D_{i,e}$ is the effective diffusivity of component i, $D_{i,K}$ is the Knudsen diffusivity of component i that can be obtained from the kinetic theory of gases,[50] $D_{i,j}$ is the binary diffusivity of component i in a mixture of i and j that can be calculated from the Chapman–Enskog equation,[51] and x_i is the mole fraction of component i. The Wilke–Bosanquet model is a very good approximation of the Dusty Gas model in this case, as proven in Supporting Information Figure S2. Besides, the Wilke–Bosanquet model is computationally less demanding. It should be noted that coke deposition can narrow pores significantly, so that restricted, "configurational" diffusion becomes important. To account for this restricted diffusion, the equation for the effective diffusivity, Eq. 5, is modified[24,25,32]:

$$D_{i,e} = \left(1 - \frac{r}{r_o}\right)^4 \frac{D_{i,M} D_{i,K}}{D_{i,M} + D_{i,K}} \quad (7)$$

The reaction rate per unit pore surface area (R_i) is obtained from the work of Li et al.[16]:

$$R_i = a \, v_i \frac{k_1 \left(P_{C_3H_8} - P_{C_3H_6} P_{H_2}/K\right)}{S_k \left(1 + K_2 P_{C_3H_6} + K_3^{0.5} P_{H_2}^{0.5}\right)^2} \quad (8)$$

Here, a represents the level of activity of the catalyst for the main reaction (for a fresh catalyst, $a = 1$; for a spent catalyst, $a < 1$), which is calculated by Eqs. 12 and 13; v_i is the stoichiometric number of component i; k_1 is the reaction rate constant of the main reaction; $S_k = 56.6$ m^2/g is the specific surface area of the Pt-Sn/Al$_2$O$_3$ catalyst[16]; K is the reaction equilibrium constant of the main reaction; K_2 and K_3 are the adsorption equilibrium constants; and $P_{C_3H_8}, P_{C_3H_6}$, and, P_{H_2} are the partial pressures of propane, propylene, and hydrogen, respectively. In Eq. 8, the values of the kinetic and thermodynamic parameters (k_1, K, K_2, and K_3), which are functions of temperature, can be found in the work by Li et al.[16]

In an inner node, due to the zero-volume assumption, Kirchhoff's Law for currents is satisfied:

$$\sum_{n=1}^{n=Z} \pi r_n^2 J_{i,n} = 0 \quad (9)$$

where Z is the pore connectivity, r_n is the radius of pore n, and $J_{i,n}$ is the diffusion flux of component i in pore n. In a boundary node, a Dirichlet boundary condition is imposed, as we only concentrate on processes inside the catalyst particle:

$$C_i = C_{i,b} \quad (10)$$

where $C_{i,b}$ is the bulk concentration of component i.

Coking and deactivation

In the pore network, coking and deactivation occur simultaneously; they affect each other in three ways, namely, through site coverage, pore narrowing, and pore blockage,[7-9] as shown in Figure 2. First, coke causes deactivation by covering active sites, which is reflected by the catalyst activity (a) in Eq. 8. Then, coke narrows pores and, subsequently, reduces the effective diffusivity ($D_{i,e}$) in Eq. 7. Finally, coke plugs pores, and some open pores become isolated from the bulk phase; meanwhile, active sites in these pores become inaccessible to reactant and products. The coke formation reaction also deactivates itself in the same three ways.

The coking rate per unit pore surface area (R_c) is adopted from the literature[16]:

$$R_c = \frac{dC_c}{dt} = a_c \frac{k_c P_{C_3H_6}}{1 + K_3 P_{H_2}} \quad (11)$$

where C_c (g/m^2) is the loading of coke in a pore channel per unit surface area; a_c is the catalyst activity for coke formation, which is described by Eqs. 12 and 13; and k_c is the reaction rate constant of the coking reaction. When assuming that the coke formation reaction and main reaction occur by a single site mechanism on the same active sites, and coke uniformly deactivates these active sites, the relation between coke loading and activity can be described by[8,32,52]:

$$a = a_c = \frac{C_{cm} - C_c}{C_{cm}} \quad (12)$$

where C_{cm} is the maximum loading of coke required to completely deactivate the active sites on the catalyst surface, which is constant for a specific catalyst. Equation 12 is a good
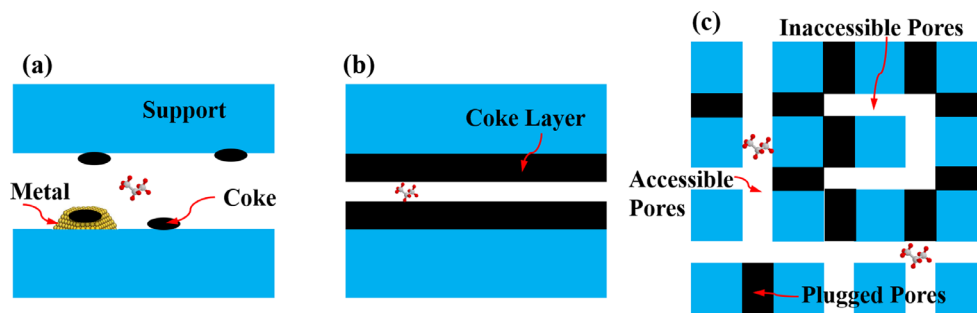
Figure 2. Mechanisms of catalyst deactivation by coke at the particle level.

(a) Site coverage, (b) pore narrowing, and (c) pore blockage. [Color figure can be viewed at wileyonlinelibrary.com]

approximation to describe the relation between coke loading and activity, as proven by Li et al.[16] Combining Eqs. 11 and 12, we can obtain:

$$-\frac{da}{dt} = a \frac{k_d P_{C_3H_6}}{1 + K_3 P_{H_2}} \quad k_d = \frac{k_c}{C_{cm}} \qquad (13)$$

where the deactivation rate constant (k_d) is a function of temperature and its value is adopted from the literature.[16]

The loading of coke at time $t + \Delta t$ is calculated by:

$$C_c(t + \Delta t) = C_c(t) + R_c(t)\Delta t \qquad (14)$$

where Δt is the time step. As coking proceeds, the pore network structure changes accordingly. The coke can accumulate on both metal sites (Pt-Sn) and support (Al$_2$O$_3$), due to the shift of the coke from metal sites to support, especially in the presence of Sn in the catalyst.[53] Thus, we assume that coke uniformly covers the pore surface, and the pore radius can be determined for a given coke loading[32]:

$$r = \sqrt{r_o^2 - 2C_c r_o / \rho_c} \qquad (15)$$

where ρ_c is the density of coke. If r is less than the molecular radius of propane (0.215 nm),[54] the pore is considered plugged by coke. Some open pores can become inaccessible to reactant and products when they are surrounded by these plugged pores (see Figure 2c). In our work, the extended Hoshen–Kopelman algorithm[55] is used to identify these inaccessible pores.

Implementation

The algorithm to solve the pore network model consists of three tightly coupled steps (see Figure 3); the details of these steps are given in the previous three subsections. In step 1, the pore network is constructed according to predefined topological and morphological parameters, and an initial guess for the concentrations is assigned to the pore network. In step 2, equations for diffusion and reaction in the pore network are solved by iteration to yield concentration profiles of reactant and products at time t, and the parameters for the pore network and catalyst activities used in this step are adopted from step 3. In step 3, equations for coking and deactivation are solved to update the pore network structure and catalyst activities at time $t + \Delta t$, in which the concentration profiles calculated in step 2 are used. If time $t + \Delta t$ does not reach the maximum time for reaction (t_m), the process returns to step 2; if time $t + \Delta t$ exceeds t_m, the results are output and the process is ended. The above algorithm is implemented in MATLAB 2010b, however, using a newer version of MATLAB can

increase the computational speed. Some data are visualized using Rhinoceros 4.0.

The solution of the pore network model yields concentration profiles of reactant, products, and coke in the pore network, as well as distributions of reaction rates for propane dehydrogenation and coke formation. With these results, the dimensionless coke content in the catalyst particle (W_c) can be calculated by[32]:

$$W_c = \frac{\text{coke content in the pore network}}{\text{maxmuim coke content}} = \frac{\sum_{n=1}^{N}(2\pi r_{o,n} l_n C_{c,n})}{\sum_{n=1}^{N}(2\pi r_{o,n} l_n C_{cm})} \qquad (16)$$

where N is the total number of pores in the pore network. As coking proceeds, W_c increases with time and the value of W_c at the end of reaction (or at the final reaction time) reflects the capacity for a catalyst particle to accommodate coke. The apparent reaction rate for propane dehydrogenation (R_{app}) can be calculated using a scaling rule[24,36]:

$$R_{app} = R_{PN} \cdot f = \sum_{n=1}^{N}(2\pi r_{o,n} l_n R_{C_3H_6,n}) \cdot \frac{S}{\sum_{n=1}^{N}(2\pi r_{o,n} l_n)} \qquad (17)$$

where R_{PN} is the overall reaction rate in the pore network, f is the thus-defined scaling factor, $R_{C_3H_6,n}$ is the formation rate of propylene in pore n, and S is the internal surface area of the catalyst particle. The decrease of R_{app} with time directly reflects the deactivation process. Meanwhile, R_{app} can also correlate with W_c, which gives the relationship between deactivation and coking.

The parameters used in the simulations are presented in Table 1. The number of nodes, 1393, is adequate and reasonable, because adding more nodes does not change the simulation results, but increases computational cost significantly (see Supporting Information Figure S3). The time step is set to 100 s to obtain accurate results and also reduce computational cost (see Supporting Information Figure S4).

Results and Discussion
Fundamental features of the coking and deactivation

An archetypical simulation is performed to probe the fundamental features of coking and deactivation in the catalyst particle for propane dehydrogenation, and the results are presented in Figure 4. Figure 4a shows that the dimensionless coke content (W_c) increases quickly at short times, but only changes
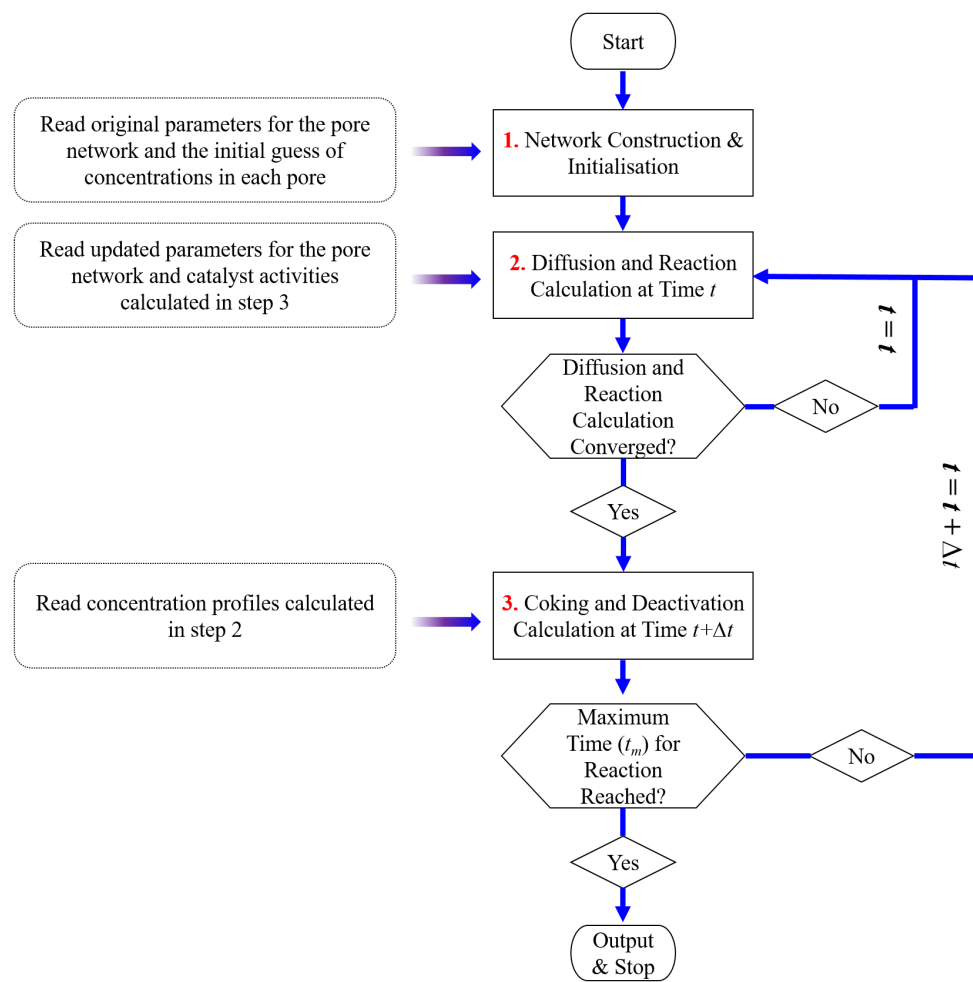
Figure 3. The algorithm for the pore network model simulating diffusion and reaction, accompanied by coking and deactivation, in a catalyst particle.

[Color figure can be viewed at wileyonlinelibrary.com]

slightly after reaching 0.40 at 2100 s, which is consistent with the trend observed in experiments.[14,15] Besides, W_c at 8000 s (i.e., 0.46) is much smaller than the maximum value (i.e., 1), indicating that the catalyst particle exhibits a poor capacity to contain coke. In Figure 4b, the apparent reaction rate (R_{app}) is correlated with W_c, and the deactivation process can be separated into two stages. R_{app} during stage 2 decreases more rapidly than during stage 1 (see Figure 4b), indicating that any

additional coke formed during stage 2 has a stronger detrimental effect on the propane dehydrogenation reaction.

To explain the results in Figure 4, distributions of coke-plugged pores, as well as concentration profiles of propane and propylene are calculated (see Figure 5). When $t \leq 1900$ s, the plugged and inaccessible pores do not form a large cluster and many pores in the central zone of the particle are still available to contain more coke; when $t \geq 2100$ s, a large cluster of plugged and inaccessible pores occupies the central zone of the particle and the number of pores available to contain coke drops sharply. This percolation phenomenon could explain the significant change in coking rate after 2100 s (see Figure 4a).

In Figure 5, the concentration gradients of propane and propylene at $t = 100$ s are very steep, indicating strong diffusion resistance in the catalyst particle. Due to diffusion limitations, the reaction rate in each pore is largely dependent on the radial position of the pore. Based on this understanding, we can infer that the coke deposited in different zones of the catalyst particle exhibits distinct toxicities to propane dehydrogenation. Specifically, if coke is preferentially deposited in the outer zone of the catalyst particle, the catalyst deactivates more quickly, because the reaction rate in this zone is much higher. When $t \geq 2100$ s, almost all the pores in the central zone of the catalyst particle become plugged or inaccessible (see

Table 1. Parameters Used in Simulations

| Number of nodes	1393
Time step (Δt)	100 s
Internal surface area of the catalyst particle (S)	100.0 m²/g
Maximum loading of coke (C_{cm})	1×10^{-3}– 8×10^{-3} g/m²
Temperature (T)	818–848 K
Total pressure (P_t)	1 bar
Bulk pressure of propane ($P_{C_3H_8,b}$)	0.5–0.8 bar
Bulk pressure of propylene ($P_{C_3H_6,b}$)	0.1–0.4 bar
Bulk pressure of hydrogen ($P_{H_2,b}$)	0.1–0.4 bar
Pore connectivity (Z)	3–6
Volume-averaged pore radius (r_a)	3.5–8 nm
Standard deviation of the natural logarithm of the pore radius (σ)	0.1–0.7
Radius of the catalyst particle (R)	0.2–4 mm
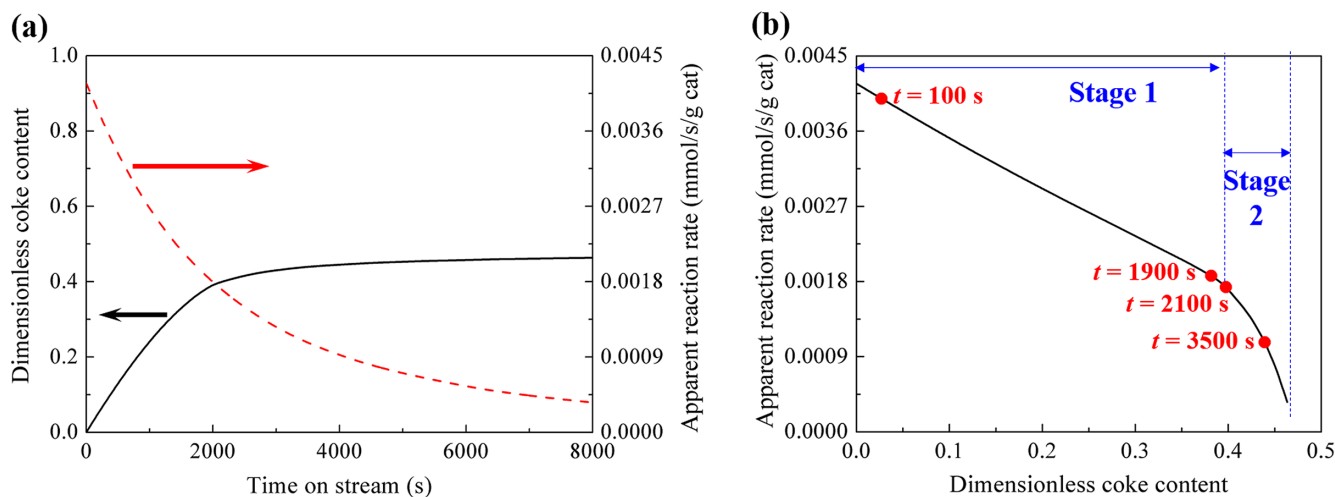
Figure 4. (a) The changes of dimensionless coke content and apparent reaction rate with time; (b) the correlation between dimensionless coke content and apparent reaction rate.

The parameters used in the simulation are: $C_{cm} = 4 \times 10^{-3}$ g/m^2, $T = 838$ K, $P_{C3H8,b} = 0.8$ bar, $P_{C3H6,b} = 0.1$ bar, $P_{H2,b} = 0.1$ bar, $Z = 4$, $r_a = 5$ nm, $\sigma = 0.5$, $R = 2$ mm. [Color figure can be viewed at wileyonlinelibrary.com]

Figure 5), which is identified by the extended Hoshen–Kopelman algorithm,[55] and then fresh coke only poisons the pores in the outer zone of the particle. This explains the stronger toxicity of the coke formed at stage 2 (see Figure 4b).

Effects of coking kinetics

The maximum loading of coke (C_{cm}) reflects the maximum capacity of a catalyst to contain coke, and this parameter is independent on the pore network structure. Figure 6a shows that the dimensionless coke content (W_c) at the final reaction time increases from 0.24 to 0.97 when changing C_{cm} from 8×10^{-3} to 1×10^{-3} g/m^2. A smaller C_{cm} indicates that less coke is produced, and hence the effect of pore blockage is less important, leading to a higher W_c. In Figure 6b, the apparent reaction rate (R_{app}) drops more rapidly with a larger C_{cm}, which is anticipated because a larger C_{cm} means a quicker coking rate according to Eq. 11, causing faster deactivation. Figure 6c shows that no obvious transition points in the curves are observed with $C_{cm} \leq 2 \times 10^{-3}$ g/m^2. In such cases, the catalyst particle is close to complete deactivation before forming a large cluster of plugged and inaccessible pores, which results in no obvious transition points. It is worth mentioning that the pore network cannot even reach the percolation threshold when C_{cm} is small enough ($\leq 1 \times 10^{-3}$ g/m^2), as shown in Supporting Information Figure S5, which explains this result.

Effects of reaction conditions

The effects of reaction temperature (T), ratio between bulk pressure of propane and hydrogen ($P_{C3H8,b}/P_{H2,b}$), and ratio between bulk pressure of propane and propylene ($P_{C3H8,b}/P_{C3H6,b}$) on coking and deactivation in the catalyst particle are presented in Figures 7–9, respectively. In Figures 7a and 8a, the initial coking rate is different when varying T and $P_{C3H8,b}/P_{H2,b}$; in Figures 7b, 8b, and 9b, the initial apparent reaction rate (R_{app}) is also distinct when changing the reaction conditions. These results can be well explained by the kinetics of coke formation and the main reaction, which are given in Eqs. 8, 11, and 12. As seen from Figure 9a, the initial coking rate is independent of $P_{C3H8,b}/P_{C3H6,b}$. This is because propane can be quickly dehydrogenated to propylene when

compared to coke formation rate and, hence, the concentration of propylene (which is the coke precursor) in the central zone of the catalyst particle changes very little (see Supporting Information Figure S8 and Figure 5). As seen from Figures 7a, 8a, and 9a, the dimensionless coke content at the final reaction time remains almost unchanged ($W_c = 0.45$–0.48). This is because reaction conditions do not change the effect of pore blockage in the catalyst particle, which is related to the percolation threshold, a geometric property. Besides, in Figure 7c, 8c, and 9c, the transition point in the curve becomes less obvious when $T \leq 818$ K, $P_{C3H8,b}/P_{H2,b} \leq 6/3$, and $P_{C3H8,b}/P_{C3H6,b} \leq 6/3$. Under these reaction conditions, the concentration gradients of reactant and product are small (see Supporting Information Figures S6–S8) and the reaction rates in all the pores are very close to each other, which leads to close toxicities of the coke deposited in different zones of the catalyst particle.

Effects of pore network structure

Pore connectivity (Z) is a principal characteristic for the topology of pore networks. The effects of Z on coking and deactivation are displayed in Figure 10. Figure 10a shows that the dimensionless coke content (W_c) at the final reaction time increases from 0.40 to 0.52 with Z changing from 3 to 6, indicating that catalysts with a smaller Z have a lower capacity to contain coke. This result is expected, because open pores in pore networks with a smaller Z are more likely to be surrounded by plugged pores and become unavailable to accommodate coke. Figure 10b shows that the initial apparent reaction rate increases when Z changes from 3 to 6, which can be attributed to the reduced diffusion resistance. As seen from Figure 10c, the transition point moves toward a higher value of W_c when increasing Z, implying that more coke is required to form a large cluster where plugged and inaccessible pores occupy the central zone of the catalyst particle.

Pore-size distribution is described by two parameters (see Eq. 1), namely, volume-averaged pore radius (r_a) and standard deviation of the natural logarithm of the pore radius (σ). In Figure 11a, the dimensionless coke content (W_c) at the final reaction time increases from 0.34 to 0.72 with r_a changing from 3.5 to 8.0 nm. Obviously, a larger r_a means that more

□ **Distributions of coke-plugged pores**
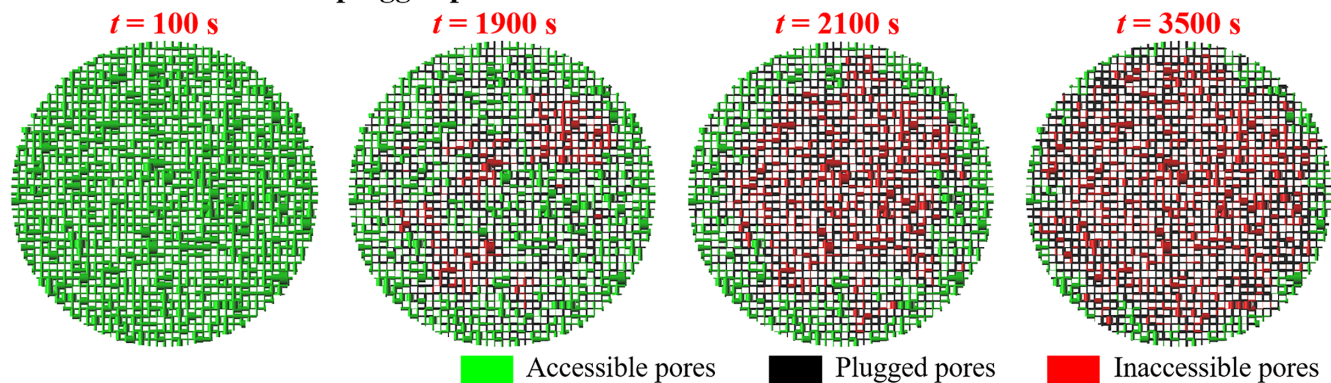
□ **Concentration profiles of propane**
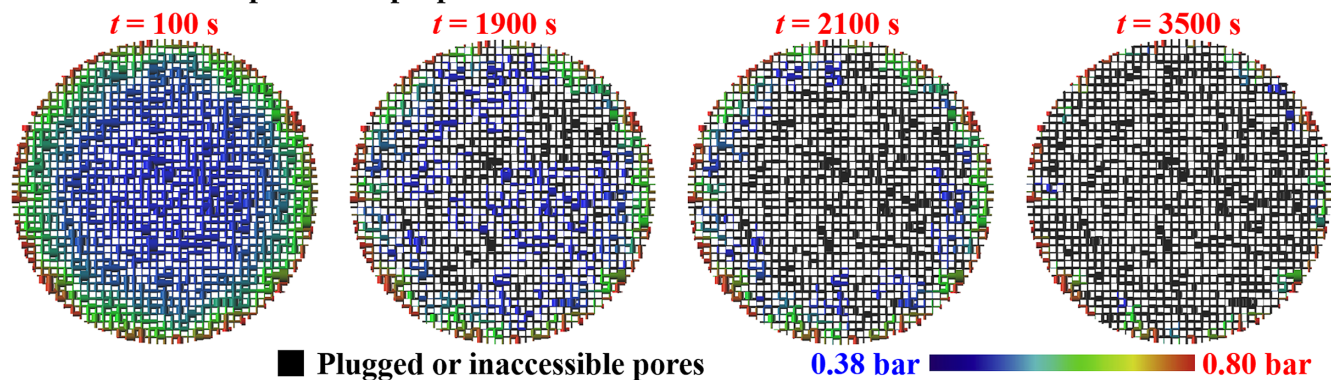
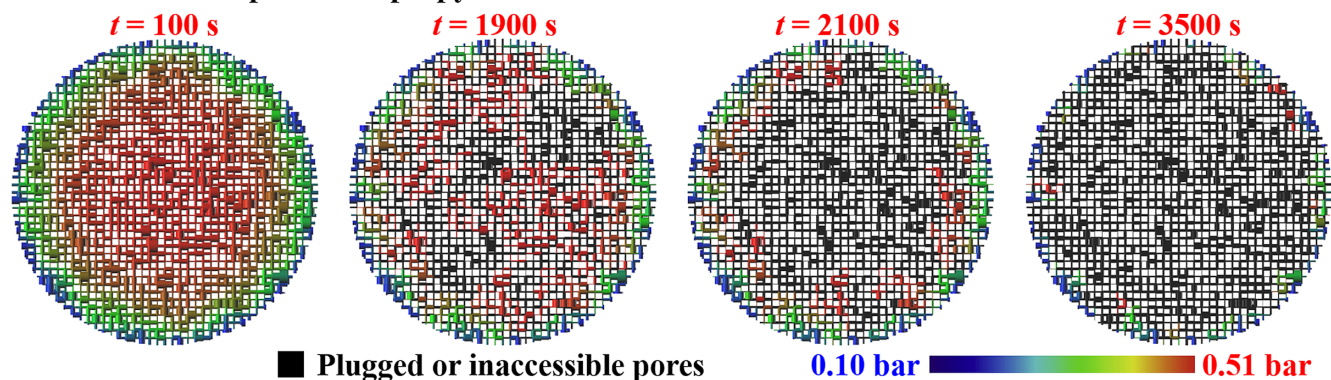□ **Concentration profiles of propylene**

Figure 5. **The distributions of coke-plugged and concentration profiles of propane and propylene in the pore network, at different times on stream.**

Accessible, plugged, and inaccessible pores are illustrated in Figure 2c. The parameters used in the simulation are: $C_{cm} = 4 \times 10^{-3}$ g/m^2, $T = 838$ K, $P_{C3H8,b} = 0.8$ bar, $P_{C3H6,b} = 0.1$ bar, $P_{H2,b} = 0.1$ bar, $Z = 4$, $r_a = 5$ nm, $\sigma = 0.5$, $R = 2$ mm. [Color figure can be viewed at wileyonlinelibrary.com]

pore volume is available to contain coke. As seen from Figure 11b, the apparent reaction rate increases with r_a, due to the reduced diffusion resistance. In Figure 11c, the transition point moves toward higher W_c when increasing r_a. More coke is needed to plug large pores, and, therefore, more coke is required to form a large cluster of plugged and inaccessible pores.

Figure 12 displays the effect of standard deviation of the natural logarithm of the pore radius (σ) on coking and deactivation. In Figure 12a, the dimensionless coke content (W_c) at the final reaction time decreases from 0.72 to 0.36 with σ increasing from 0.1 to 0.7. A higher σ means a broader distribution of pore radii and also implies a larger percentage of

small pores. In this case, large pores are more likely to be surrounded by plugged small pores and subsequently become inaccessible, resulting in the decreased W_c. Figure 12b shows that the apparent reaction rate decreases with the increase of σ from 0.1 to 0.7, which is anticipated, because the diffusion resistance is larger for a broader pore-size distribution. Figure 12c shows that the transition point moves toward low W_c when increasing σ. This is because less coke is needed to form a large cluster of plugged and inaccessible pores when the pore-size distribution is broader.

Figure 13 presents the effects of particle radius (R) on coking and deactivation. As seen from Figure 13a, the initial coking rate increases with R changing from 0.5 to 4.0 mm.
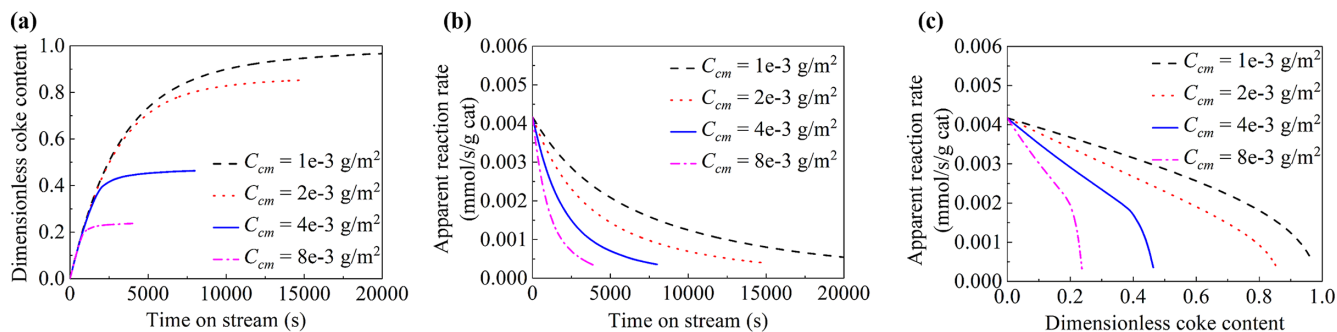
Figure 6. Effects of maximum loading of coke (C_{cm}) on: (a) dimensionless coke content, (b) apparent reaction rate, and (c) the relation between apparent reaction rate and dimensionless coke content.

The parameters used in the simulation are: T = 838 K, $P_{C3H8,b}$ = 0.8 bar, $P_{C3H6,b}$ = 0.1 bar, $P_{H2,b}$ = 0.1 bar, Z = 4, r_a = 5 nm, σ = 0.5, R = 2 mm. [Color figure can be viewed at wileyonlinelibrary.com]
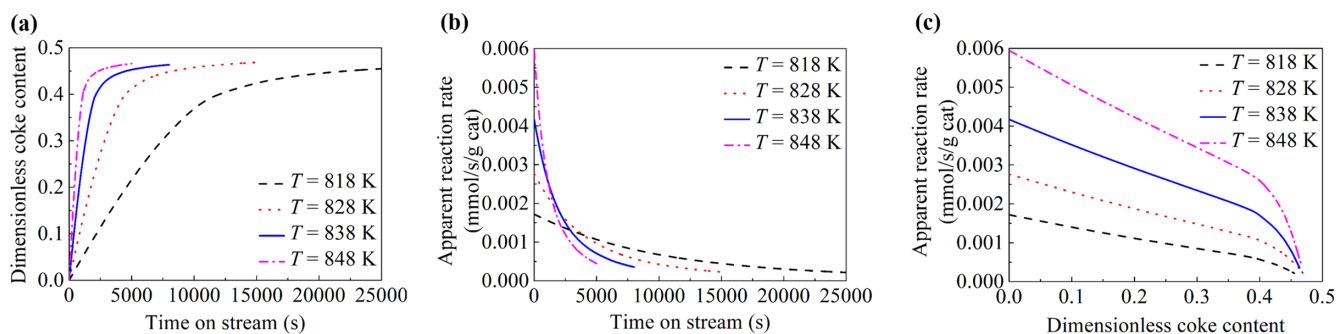

Figure 7. Effects of reaction temperature (T) on: (a) dimensionless coke content, (b) apparent reaction rate, and (c) the relation between apparent reaction rate and dimensionless coke content.

The parameters used in the simulation are: C_{cm} = 4 × 10^{-3} g/m^2, $P_{C3H8,b}$ = 0.8 bar, $P_{C3H6,b}$ = 0.1 bar, $P_{H2,b}$ = 0.1 bar, Z = 4, r_a = 5 nm, σ = 0.5, R = 2 mm. [Color figure can be viewed at wileyonlinelibrary.com]
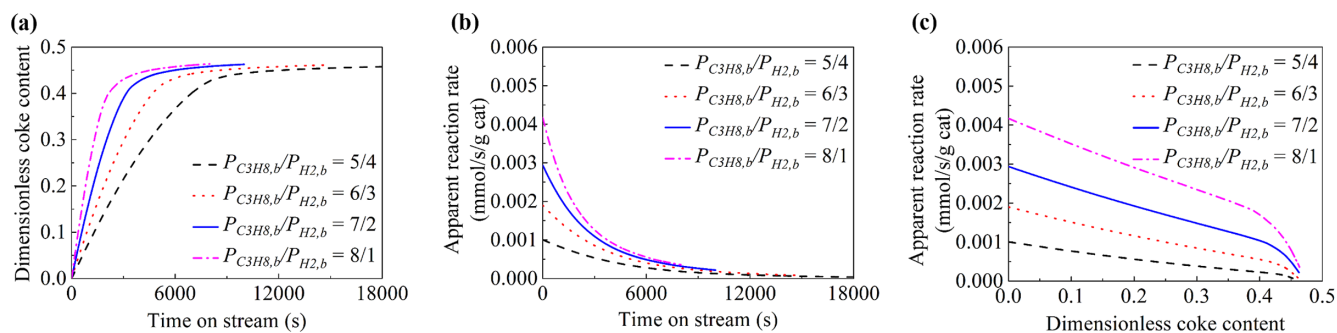

Figure 8. Effects of the ratio of the bulk pressure of propane to that of hydrogen ($P_{C3H8,b}/P_{H2,b}$) on: (a) dimensionless coke content, (b) apparent reaction rate, and (c) the relation between apparent reaction rate and dimensionless coke content.

The parameters used in the simulation are: C_{cm} = 4 × 10^{-3} g/m^2, T = 838 K, P_t = 1 bar, $P_{C3H6,b}$ = 0.1 bar, Z = 4, r_a = 5 nm, σ = 0.5, R = 2 mm. [Color figure can be viewed at wileyonlinelibrary.com]

The concentrations of propylene (coke precursor) in the pores are lower for smaller catalyst particles (see Supporting Information Figure S9 and Figure 5), and, therefore, the coking rate is reduced according to Eq. 11. Besides, Figure 13a also shows that the dimensionless coke content at the final reaction time does not change with the particle radius, which indicates that the pore radius does not affect the capacity for a catalyst particle to contain coke. In Figure 13b, the apparent reaction rate decreases with the increase of R from 0.5 to 4.0 mm, which is expected, because the diffusion path is lengthened.

Figure 13c shows that the transition point becomes less obvious when R < 0.5 mm. The concentration gradients of reactant and product are small when R = 0.5 mm (see Supporting Information Figure S9), leading to very close toxicities of coke deposited along different radial zones of the catalyst particle.

Conclusions

A pore network model is proposed to simulate coupled diffusion, reaction, coking, and deactivation in the Pt-Sn/Al$_2$O$_3$
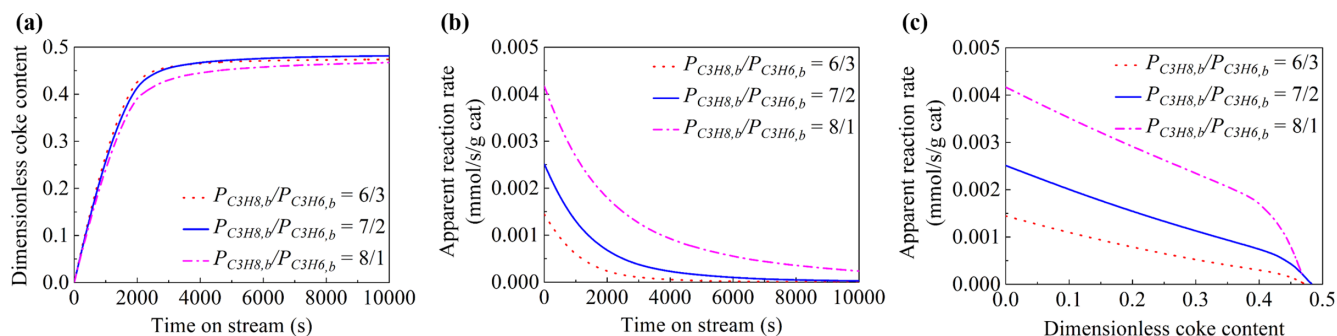
Figure 9. Effects of the ratio of the bulk pressure of propane to that of propylene ($P_{C3H8,b}/P_{C3H6,b}$) on: (a) dimensionless coke content, (b) apparent reaction rate, and (c) the relation between apparent reaction rate and dimensionless coke content.

The parameters used in the simulation are: $C_{cm} = 4 \times 10^{-3}$ g/m^2, $T = 838$ K, $P_t = 1$ bar, $P_{H2,b} = 0.1$ bar, $Z = 4$, $r_a = 5$ nm, $\sigma = 0.5$, $R = 2$ mm. [Color figure can be viewed at wileyonlinelibrary.com]
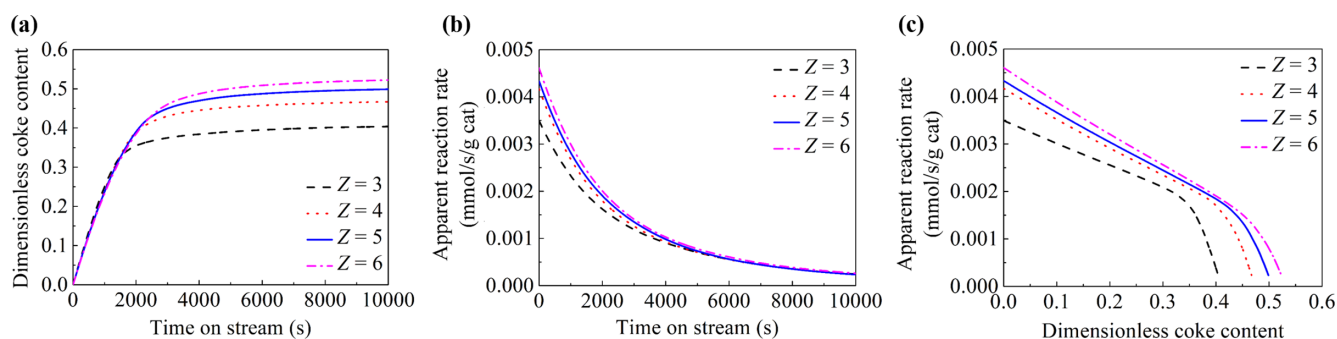

Figure 10. Effects of pore connectivity (Z) on: (a) dimensionless coke content, (b) apparent reaction rate, and (c) the relation between apparent reaction rate and dimensionless coke content.

The parameters used in the simulation are: $C_{cm} = 4 \times 10^{-3}$ g/m^2, $T = 838$ K, $P_{C3H8,b} = 0.8$ bar, $P_{C3H6,b} = 0.1$ bar, $P_{H2,b} = 0.1$ bar, $r_a = 5$ nm, $\sigma = 0.5$, $R = 2$ mm. [Color figure can be viewed at wileyonlinelibrary.com]
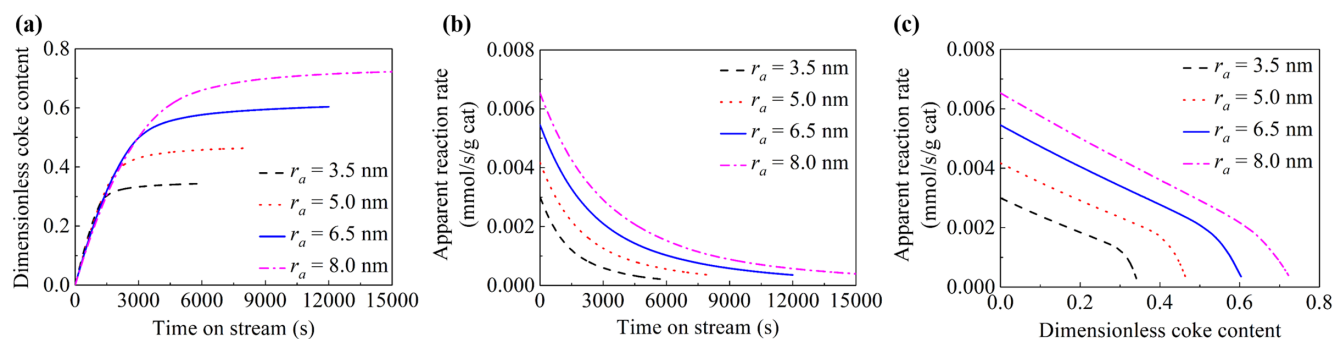

Figure 11. Effects of volume-averaged pore radius (r_a) on: (a) dimensionless coke content, (b) apparent reaction rate, and (c) the relation between apparent reaction rate and dimensionless coke content.

The parameters used in the simulation are: $C_{cm} = 4 \times 10^{-3}$ g/m^2, $T = 838$ K, $P_{C3H8,b} = 0.8$ bar, $P_{C3H6,b} = 0.1$ bar, $P_{H2,b} = 0.1$ bar, $Z = 4$, $\sigma = 0.5$, $R = 2$ mm. [Color figure can be viewed at wileyonlinelibrary.com]

catalyst particle for propane dehydrogenation. Three deactivation mechanisms are accounted for, namely, site coverage, pore narrowing, and pore blockage. The general features of coking and deactivation for propane dehydrogenation are obtained by analyzing an archetypical simulation. Then, the effects of coking kinetics (maximum loading of coke), reaction conditions (temperature, $P_{C_3H_8,b}/P_{H_2,b}$, and $P_{C_3H_8,b}/P_{C_3H_6,b}$), and pore network structure (connectivity, pore-size distribution, and particle radius) on coking and deactivation are investigated.

The deactivation process in the catalyst particle for propane dehydrogenation can be divided into two stages where the toxicity of coke in the later stage is much stronger than of coke in the early stage. This difference in coke toxicity is attributed to pore blockage and diffusion limitations, as explained by analyzing distributions of coke, as well as concentration profiles of propane and propylene. The maximum loading of coke in the coking kinetics affects coke formation rate and, subsequently, influences the deactivation process in the catalyst particle. The reaction conditions significantly affect coking rate
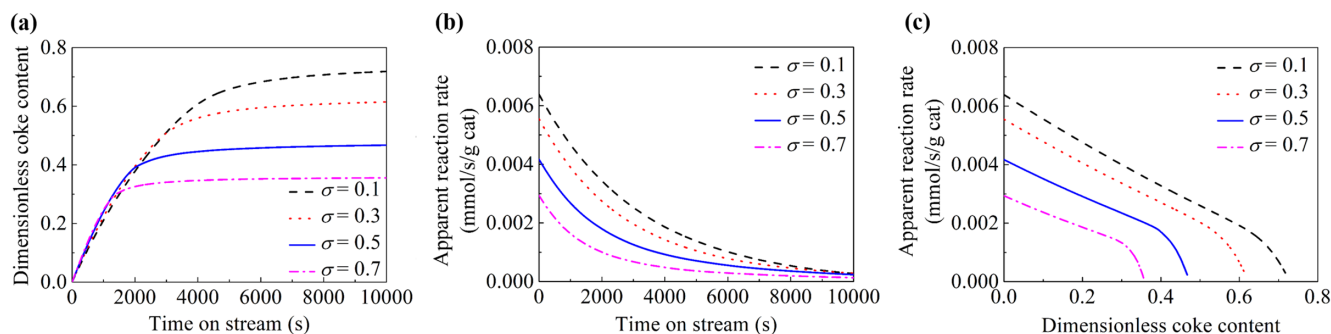
Figure 12. Effects of standard deviation of the natural logarithm of the pore radius (σ) on: (a) dimensionless coke content, (b) apparent reaction rate, and (c) the relation between apparent reaction rate and dimensionless coke content.

The parameters used in the simulation are: $C_{cm} = 4 \times 10^{-3}$ g/m^2, $T = 838$ K, $P_{C3H8,b} = 0.8$ bar, $P_{C3H6,b} = 0.1$ bar, $P_{H2,b} = 0.1$ bar, $Z = 4$, $r_a = 5$ nm, $R = 2$ mm. [Color figure can be viewed at wileyonlinelibrary.com]
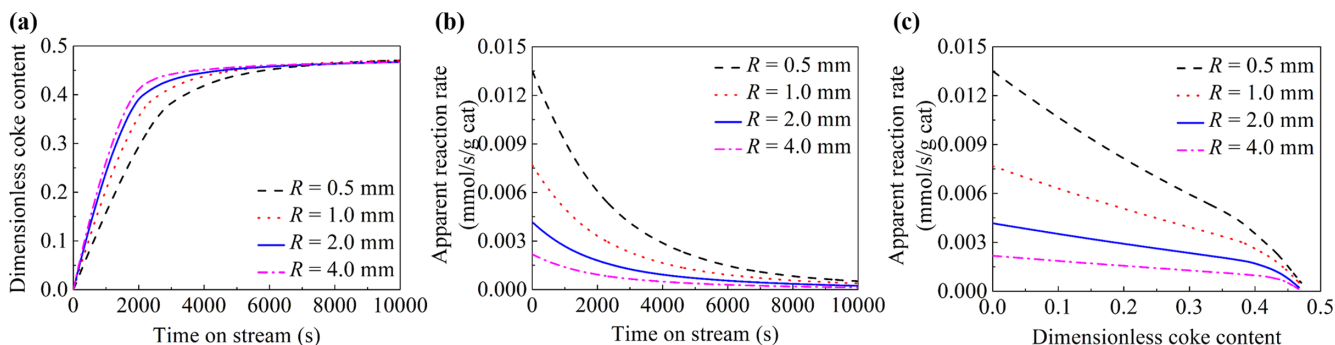

Figure 13. Effects of particle radius (R) on: (a) dimensionless coke content, (b) apparent reaction rate, and (c) the relation between apparent reaction rate and dimensionless coke content.

The parameters used in the simulation are: $C_{cm} = 4 \times 10^{-3}$ g/m^2, $T = 838$ K, $P_{C3H8,b} = 0.8$ bar, $P_{C3H6,b} = 0.1$ bar, $P_{H2,b} = 0.1$ bar, $Z = 4$, $r_a = 5$ nm, $\sigma = 0.5$. [Color figure can be viewed at wileyonlinelibrary.com]

and the apparent rate of the main reaction, but they do not change the capacity for a catalyst particle to contain coke. The pore network structure influences the apparent reaction rate considerably by changing the diffusion resistance and diffusion path length. A catalyst particle with higher connectivity, larger volume-averaged pore radius, and narrower pore-size distribution has a higher capacity to contain coke. However, the particle radius does not affect the capacity of a catalyst particle to accommodate coke. These results should be used to guide the rational design of robust catalysts against deactivation by coke formation.

Acknowledgments

Literature Cited

1. Sattler JJHB, Ruiz-Martinez J, Santillan-Jimenez E, Weckhuysen BM. Catalytic dehydrogenation of light alkanes on metals and metal oxides. *Chem Rev*. 2014;114:10613-10653.

2. Carrero CA, Schloegl R, Wachs IE, Schomaecker R. Critical literature review of the kinetics for the oxidative dehydrogenation of propane over well-defined supported vanadium oxide catalysts. *ACS Catal*. 2014;4:3357-3380.

3. Corma A, Melo FV, Sauvanaud L, Ortega F. Light cracked naphtha processing: controlling chemistry for maximum propylene production. *Catal Today*. 2005;107–108:699-706.

4. Galvis Hirsa MT, de Jong KP. Catalysts for production of lower olefins from synthesis gas: a review. *ACS Catal*. 2013;3:2130-2149.

5. Nawaz Z. Light alkane dehydrogenation to light olefin technologies: a comprehensive review. *Rev Chem Eng*. 2015;31:413-436.

6. Bhasin MM, McCain JH, Vora BV, Imai T, Pujadó PR. Dehydrogenation and oxydehydrogenation of paraffins to olefins. *Appl Catal Gen*. 2001;221:397-419.

7. Froment GF. Coke formation in catalytic processes: kinetics and catalyst deactivation. *Stud Surf Sci Catal*. 1997;111:53-68.

8. Froment GF. Modeling of catalyst deactivation. *Appl Catal Gen*. 2001; 212:117-128.

9. Froment GF. Kinetic modeling of hydrocarbon processing and the effect of catalyst deactivation by coke formation. *Catal Rev*. 2008;50: 1-18.

10. Chrysostomou D, Zaera F. Thermal chemistry of C3 allyl groups on Pt(111). *J Phys Chem B*. 2001;105:1003-1011.

11. Otero G, González C, Pinardi AL, et al. Ordered vacancy network induced by the growth of epitaxial graphene on Pt(111). *Phys Rev Lett*. 2010;105:216102.

12. Yang M-L, Zhu Y-A, Zhou X-G, Sui Z-J, Chen D. First-principles calculations of propane dehydrogenation over PtSn catalysts. *ACS Catal*. 2012;2:1247-1258.

13. Yang M-L, Zhu Y-A, Fan C, Sui Z-J, Chen D, Zhou X-G. DFT study of propane dehydrogenation on Pt catalyst: effects of step sites. *Phys Chem Chem Phys*. 2011;13:3257-3267.

14. Van Sint Annaland M, Kuipers JAM, Van Swaaij WPM. A kinetic rate expression for the time-dependent coke formation rate during propane dehydrogenation over a platinum alumina monolithic catalyst. *Catal Today*. 2001;66:427-436.

15. Lobera MP, Tellez C, Herguido J, Menendez M. Transient kinetic modelling of propane dehydrogenation over a Pt-Sn-K/Al$_2$O$_3$ catalyst. *Appl Catal Gen*. 2008;349:156-164.

16. Li Q, Sui Z, Zhou X, Chen D. Kinetics of propane dehydrogenation over Pt-Sn/Al$_2$O$_3$ catalyst. *Appl Catal Gen*. 2011;398:18-26.

17. Larsson M, Henriksson N, Andersson B. Investigation of the kinetics of a deactivating system by transient experiments. *Appl Catal Gen*. 1998;166:9-19.

18. Gascón J, Téllez C, Herguido J, Menéndez M. Propane dehydrogenation over a Cr$_2$O$_3$/Al$_2$O$_3$ catalyst: transient kinetic modeling of propene and coke formation. *Appl Catal Gen*. 2003;248:105-116.

19. Behnam M, Dixon AG, Nijemeisland M, Stitt EH. Catalyst deactivation in 3D CFD resolved particle simulations of propane dehydrogenation. *Ind Eng Chem Res*. 2010;49:10641-10650.

20. Gascon J, Tellez C, Herguido J, Jakobsen HA, Menendez M. Modeling of fluidized bed reactors with two reaction zones. *AIChE J*. 2006;52:3911-3923.

21. Gascon J, Tellez C, Herguido J, Menendez M. A two-zone fluidized bed reactor for catalytic propane dehydrogenation. *Chem Eng J*. 2005;106:91-96.

22. Lobera MP, Tellez C, Herguido J, Menendez M. Propane dehydrogenation over Pt-Sn-K/γ-Al$_2$O$_3$ catalyst in a two-zone fluidized bed reactor. *Ind Eng Chem Res*. 2008;47:9314-9320.

23. Nawaz Z, Chu Y, Yang W, Tang X, Wang Y, Wei F. Study of propane dehydrogenation to propylene in an integrated fluidized bed reactor using Pt-Sn/Al-SAPO-34 novel catalyst. *Ind Eng Chem Res*. 2010;49:4614-4619.

24. Keil FJ, Rieckmann C. Optimization of three-dimensional catalyst pore structures. *Chem Eng Sci*. 1994;49:4811-4822.

25. Rao SM, Coppens M-O. Increasing robustness against deactivation of nanoporous catalysts by introducing an optimized hierarchical pore network- application to hydrodemetalation. *Chem Eng Sci*. 2012;83:66-76.

26. Rao SM, Coppens M-O. Mitigating deactivation effects through rational design of hierarchically structured catalysts: application to hydrodemetalation. *Ind Eng Chem Res*. 2010;49:11087-11097.

27. Vogelaar BM, Berger RJ, Bezemer B, et al. Simulation of coke and metal deposition in catalyst pellets using a non-steady state fixed bed reactor model. *Chem Eng Sci*. 2006;61:7463-7478.

28. Beeckman JW, Froment GF. Deactivation of catalysts by coke formation in the presence of internal diffusional limitation. *Ind Eng Chem Fundam*. 1982;21:243-250.

29. Arbabi S, Sahimi M. Computer simulations of catalyst deactivation-II. The effect of morphological, transport and kinetic parameters on the performance of the catalyst. *Chem Eng Sci*. 1991;46:1749-1755.

30. Arbabi S, Sahimi M. Computer simulations of catalyst deactivation-I. model formulation and validation. *Chem Eng Sci*. 1991;46:1739-1747.

31. Moulijn JA, van Diepen AE, Kapteijn F. Catalyst deactivation: is it predictable? What to do? *Appl Catal A Gen*. 2001;212:3-16.

32. Biswas J, Do DD. A unified theory of coking deactivation in a catalyst pellet. *Chem Eng J*. 1987;36:175-191.

33. Chigada PI, Wang J, Al-duri B, Wood J, Rigby SP. Modelling of pore structure evolution during catalyst deactivation and comparison with experiment. *Chem Eng Sci*. 2010;65:5550-5558.

34. Sahimi M, Gavalas GR, Tsotsis TT. Statistical and continuum models of fluid-solid reactions in porous media. *Chem Eng Sci*. 1990;45:1443-1502.

35. Stauffer D. *Introduction to Percolation Theory*. London: Taylor and Francis; 1985.

36. Keil F. Diffusion and reaction in porous networks. *Catal Today*. 1999;53:245-258.

37. Zhang L, Seaton NA. The application of continuum equations to diffusion and reaction in pore networks. *Chem Eng Sci*. 1994;49:41-50.

38. Beeckman JW, Froment GF. Catalyst deactivation by site coverage and blockage: finite rate of growth of the carbonaceous deposit. *Chem Eng Sci*. 1980;35:805-815.

39. Hollewand MP, Gladden LF. Modelling of diffusion and reaction in porous catalysts using a random three-dimensional network model. *Chem Eng Sci*. 1992;47:1761-1770.

40. Ye G, Sun Y, Zhou X, Zhu K, Zhou J, Coppens M-O. Method for generating pore networks in porous particles of arbitrary shape, and its application to catalytic hydrogenation of benzene. *Chem Eng J*. 2017;329:56-65.

41. Wood J, Gladden LF, Keil FJ. Modelling diffusion and reaction accompanied by capillary condensation using three-dimensional pore networks. Part 2. Dusty gas model and general reaction kinetics. *Chem Eng Sci*. 2002;57:3047-3059.

42. Wood J, Gladden LF. Modelling diffusion and reaction accompanied by capillary condensation using three-dimensional pore networks. Part 1. Fickian diffusion and pseudo-first-order reaction kinetics. *Chem Eng Sci*. 2002;57:3033-3045.

43. Ye G, Zhou X, Coppens M-O, Zhou J, Yuan W. Influence of catalyst pore network structure on the hysteresis of multiphase reactions. *AIChE J*. 2017;63:78-86.

44. Ye G, Zhou X, Coppens M-O, Yuan W. Probing pore blocking effects on multiphase reactions within porous catalyst particles using a discrete model. *AIChE J*. 2016;62:451-460.

45. Dadvar M, Sahimi M. Pore network model of deactivation of immobilized glucose isomerase in packed-bed reactors II: three-dimensional simulation at the particle level. *Chem Eng Sci*. 2002;57:939-952.

46. Dadvar M, Sahimi M. Pore network model of deactivation of immobilized glucose isomerase in packed-bed reactors. Part III: multiscale modelling. *Chem Eng Sci*. 2003;58:4935-4951.

47. Chua LM, Vazhnova T, Mays TJ, Lukyanov DB, Rigby SP. Deactivation of PtH-MFI bifunctional catalysts by coke formation during benzene alkylation with ethane. *J Catal*. 2010;271:401-412.

48. Marin GB, Beeckman JW, Froment GF. Rigorous kinetic models for catalyst deactivation by coke deposition: application to butene dehydrogenation. *J Catal*. 1986;97:416-426.

49. Murray KL, Seaton NA, Day MA. Use of mercury intrusion data, combined with nitrogen adsorption measurements, as a probe of pore network connectivity. *Langmuir*. 1999;15:8155-8160.

50. Welty JR, Wicks CE, Wilson RE, Rorrer GL. *Fundamentals of Momentum, Heat and Mass Transfer*. 5th ed. Hoboken: John Wiley & Sons; 2008.

51. Poling BE, Prasunitz JM, O'Connell JP. *The Properties of Gases and Liquids*. 5th ed. Boston, MA: McGraw-Hill; 2001.

52. Beeckman J, Froment G. Catalyst deactivation by active site coverage and pore blockage. *Ind Eng Chem Fundam*. 1979;18:245-256.

53. Larsson M, Hulten M, Blekkan EA, Andersson B. The effect of reaction conditions and time on stream on the coke formed during propane dehydrogenation. *J Catal*. 1996;164:44-53.

54. Ruthven DM. *Principles of Adsorption and Adsorption Processes*. John Wiley & Sons; 1984.

55. Al-Futaisi A, Patzek TW. Extension of Hoshen–Kopelman algorithm to non-lattice environments. *Physica A*. 2003;321:665-678.